CRYSTAL GROWTH & DESIGN

Article

pubs.acs.org/crystal

Thermochemistry of Racemic and Enantiopure Organic Crystals for Predicting Enantiomer Separation

Hannes K. Buchholz,[†,#] Rebecca K. Hylton,[†,‡,#] Jan Gerit Brandenburg,[‡] Andreas Seidel-Morgenstern,[†] Heike Lorenz,[†] Matthias Stein,[*,†] and Sarah L. Price[*,‡]

[†]Max Planck Institute for Dynamics of Complex Technical Systems, Sandtorstrasse 1, 39106 Magdeburg, Germany

[‡]Department of Chemistry, University College London, 20 Gordon Street, London WC1H 0AJ, U.K.

Supporting Information

ABSTRACT: The separation of an enantiomer from a racemic mixture is of primary relevance to the pharmaceutical industry. The thermochemical properties of organic enantiopure and racemate crystals can be exploited to design an enantioselective crystallization process. The thermodynamic difference between the two crystal forms is accessible by two cycles which give the eutectic composition in solution. The "sublimation cycle" requires calculating the lattice energy and phonon frequencies of the crystal structures. Experimental results from heat capacity and other thermodynamic measurements of enantiopure and racemic crystals are compared with a variety of molecular and crystal structure-based calculations. This is done for three prototypes of pharmaceutical-like molecules with different degrees of molecular flexibility. Differences in crystal packing result in varying temperature-dependent heat capacities and affect the sublimation thermodynamics, relative solubility, and eutectic composition. Many simplifying assumptions about the thermodynamics and solubilities of the racemic and enantiopure crystals are critically evaluated. We show that calculations and experimental information using the sublimation cycle can guide the design of processes to resolve enantiomers by crystallization.

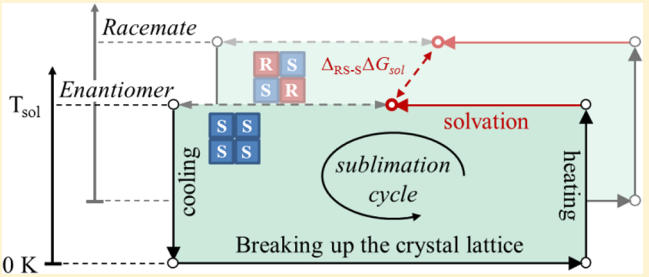

1. INTRODUCTION

New pharmaceuticals are predominantly chiral compounds but often are synthesized as racemates, i.e., an equimolar mixture of two enantiomers.[1] Despite identical chemical structures, the two mirror images display different pharmacological, toxicological, and pharmacokinetic properties. Chiral separation of these compounds or proof of harmlessness of the inactive enantiomer is now required for drug product approval[2] and is gaining importance also in the agrochemical sector.[3] There are different processes to separate enantiomers, but, if possible, crystallization is usually the preferred method for manufacture.[4] Crystallization-based separation of enantiomers leads to pure crystalline enantiomers, and recent computational estimates suggest[5] that it may be applicable to more systems if the molecular basis were fully understood. Such an enantioselective crystallization process depends on the ternary phase diagram between crystalline enantiomer, racemate, and solvent when crystallization is driven by thermodynamic control. The key parameters to a successful process are the solubilities of the pure enantiomer and the racemate, the composition of the eutectic system in the given solvent (mixture), and temperature. The eutectic composition, defined as the maximum solubility of one enantiomer in the presence of the second (see Supporting Information, Figure S1), $x_{eu} = x_S^{eu}/(x_S^{eu} + x_R^{eu})$ can be a function of temperature, T, and solvent.[6,7] In some cases shifts in the composition at the eutectic ("eutectic shifts") can vary sufficiently with temperature to allow separation by a two-step crystallization process.[7] Polymorphism and the formation of solvates further complicate advanced process design. In early stages of drug development, it is desirable to have computational methods to support, or possibly replace, many experimental investigations. The difference in solution free energies $\Delta_{RS-S}\Delta G_{sol}$ determines the enantiomeric enrichment. ΔG_{sol} can, in principle, be obtained from two hypothetical thermodynamic cycles[8,9] (see Figure 1):

(i) transfer of the molecule from crystal to the supercooled melt and then exchange of molecules between the melt and solvent, and

(ii) transfer of the molecule from crystal to vapor and then into solution.

Cycle (i), the "melt cycle", requires knowledge of the melting temperature and enthalpy of melting for determining the Gibbs free energy of melting via $\Delta G_{melt} = \Delta H_{melt} - T\,\Delta H_{melt}/T_{melt}$ plus thermal contributions of the solid and the supercooled melt (see Figure 1).

This approach is used by the general solubility equation (GSE),[10−12] other QSPR methods,[13] and by activity coefficient based models.[14] Several organic compounds already decompose before or during melting, which poses a severe restriction on its

Received: April 24, 2017
Revised: July 3, 2017
Published: July 18, 2017

DOI: 10.1021/acs.cgd.7b00582
Cryst. Growth Des. 2017, 17, 4676−4686

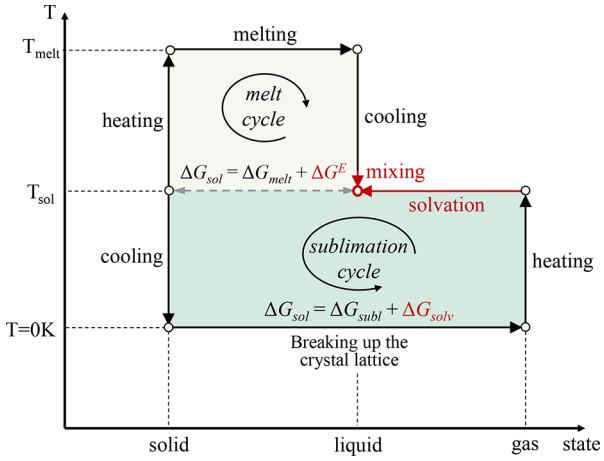

Figure 1. Two thermodynamic cycles to obtain the free energy of solution ΔG_{sol}. The melt cycle relies on the free energy of melting, ΔG_{melt}, and on the free energy of mixing $\Delta G^E = RT \ln \gamma$. The sublimation cycle uses the free energies of sublimation ΔG_{subl}, and the solvation free energy ΔG_{solv}. Solvent-dependent properties are in red.

applicability as the melting properties can only be predicted computationally by group contribution or QSPR methods which cannot distinguish between polymorphs or chiral molecules.[15,16] The other major term, the partial molar Gibbs free energy of mixing the solvent with the supercooled melt, is accessible by correlative activity coefficient and predictive based models (g^E-models)[14,17,18] Cycle (ii), the "sublimation cycle", the focus of this paper, approximates the solubility differences by taking the molecule from the crystal to the gas phase and then into solution.

Both cycles consider properties from the crystals (melting or sublimation free energy) and are thus dependent on the crystal structures of the racemate and enantiomer. The sublimation cycle is preferred as it makes use of the computationally accessible thermodynamics states from the gas and the crystalline solid.

The "sublimation cycle" has been evaluated for the computational prediction of the solubility[19] and sublimation free energies of organic crystals.[20] Here, we evaluate the sublimation cycle to obtain differences in solubilities of the racemic and enantiopure crystals and to assess the relevance of differences in thermodynamic terms which are often taken to be negligible. In the sublimation cycle, the mole fraction solubility, x, is directly related to the Gibbs free energy of solution[21−23] and can be calculated from the sublimation and solvation free energies (lower part of Figure 1).

$$-RT\ln x = \Delta G_{sol} = \Delta G_{subl} + \Delta G_{solv} \quad (1)$$

Assuming that there is no polymorphic phase transition between 0 K and the temperature of interest, T, (e.g., the solution temperature), the sublimation free energy is given by

$$\Delta G_{subl} = \Delta H_{subl} - \Delta TS_{subl} = -E_{latt} + H_{corr} - T\Delta S_{subl}$$

$$\text{with } H_{corr} = (E^g_{ZPE} - E^s_{ZPE}) + \int_{T'=0}^{T} \Delta C_P^{g-s}(T')\,dT'$$

$$\text{and } T\Delta S_{subl} = T\int_{T'=0}^{T} \frac{\Delta C_P^{g-s}(T')}{T'}\,dT' \quad (2)$$

where E_{latt} is the lattice energy, E_{ZPE} is the zero-point vibrational energy and $C_P^{g-s}(T) = C_P^g(T) - C_P^s(T)$ is the temperature-dependent isobaric heat capacity difference between the gas (g) and solid (s). The term H_{corr} is the sum of the zero-point energies (ZPEs) and the integrals of C_P and is often referred to as the "thermal correction". Thus, calculations of the solubility will not only be dependent on the accuracy of the lattice energy calculations, but also on that of other contributions to the thermodynamic cycles.[19]

The molecules investigated in this study (Figure 2) were chosen to represent prototypes of frequently occurring organic

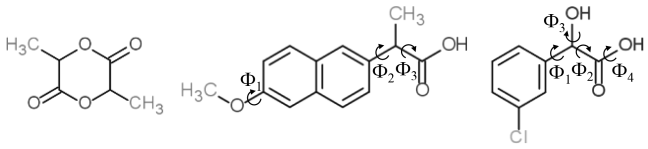

Figure 2. Molecular structures of the three representative chiral molecules: (left) 3,6-dimethyl-1,4-dioxane-2,5-dione (lactide $C_6H_8O_4$), (middle) naproxen $C_{14}H_{14}O_3$, (right) 3-chloromandelic acid (3ClMA, $C_8H_7O_3Cl$). The most flexible torsion angles are marked.

crystalline compound classes: an almost rigid molecule with no hydrogen bonding capability (lactide), a drug molecule with intermediate flexibility but only one hydrogen bonding group (naproxen), and a molecule with considerable flexibility and competing hydrogen bond donors close to the chiral center (3-chloromandelic acid).

The lactide is an internal cyclic ester of lactic acid. Both the racemic molecular compound and the (*S*)-enantiomer are used in the preparation of polylactide,[24,25] a biologically decomposable polymer with many complex properties that make it ideal for medical applications.[26] Naproxen is marketed in the enantiopure form as a nonsteroidal anti-inflammatory drug, although the racemic form is more stable.[27,28] 3-Chloromandelic acid (3ClMA) is used as an intermediate for pharmaceutical products and represents the mandelic acid family of prototypical chiral molecules.[29] It has complex polymorphic crystallization behavior that defies many current assumptions.[29,30]

Temperature-dependent heat capacities for the enantiopure and racemic crystals were determined experimentally and by computational methods for these substances. This experimental comparison is rare, with most examples being zwitterionic amino acids.[31−37] Assuming that the eutectic composition is under thermodynamic control,[6,38,39] we use a variety of experimental thermodynamic measurements and the "sublimation cycle" to evaluate whether current computational approaches can predict the eutectic composition. We critically assess the underlying assumptions that are being made to make the calculations feasible. The dominant contribution of breaking up the crystal lattice is the lattice energy, E_{latt}. The lattice energy has been widely used for understanding and modeling the organic solid state,[40−44] but improvements in modeling E_{latt} show that relative finite temperature thermodynamic properties, arising from the molecular motion, are relevant. We are assessing first the separated model ψ_{mol} for which molecular vibrations are assumed to be the same in the gas and both crystals, and so the rigid-body lattice modes can be used.[45,46] This requires electronic structure calculations on the isolated molecule only, as these can be used to define an intermolecular potential for modeling the crystals. The second recognizes that crystal packing can modify both molecular and phonon lattice modes.[47] Calculating the coupled vibrational modes is dependent on the potential energy surface for nuclear

DOI: 10.1021/acs.cgd.7b00582
Cryst. Growth Des. 2017, 17, 4676−4686

motion within the crystal, and hence the use of periodic electronic structure calculations ψ_{crys}. Dispersion corrected density functional methods, which have been widely used for lattice energies, proved to be too computationally demanding to obtain converged phonon frequencies across the Brillouin zone,[48,49] so more approximate electronic structure methods have been used. We critically assess the accuracy of the underlying assumptions against carefully determined experimental thermodynamic for chiral compounds, rarely available in early stage drug development. This study indicates that the combination of computation and experimental data can assist the design of enantiomeric separation crystallization processes but also points to the challenges in computational process design.

2. BASIC THERMODYNAMIC MODELS

In the following we briefly introduce the framework for the computation of the solid-state thermodynamic quantities and its application within a thermodynamic model to predict the eutectic composition of chiral compound-forming systems in solution.

2.1. The Solution Thermodynamics of Chiral Systems. The eutectic composition x_{eu} can be estimated as a function of the solubility ratio between the racemic compound and the enantiomer $\alpha = x_{RS}/x_S$ (see Supporting Information, pp S2−S4)[6] via the difference in Gibbs free energy of solution between the racemic compound and the enantiomer, $\Delta_{RS\text{-}S}\Delta G_{sol} = \Delta G_{sol,RS} - \Delta G_{sol,S}$, to give

$$x_{eu} = \frac{1}{1 + \alpha^2/4} = \frac{1}{1 + 1/4 \exp\left(-2\frac{\Delta_{RS-S}\Delta G_{sol}}{RT}\right)} \quad (3)$$

This derivation differs in the reference state used from a previously proposed model (see Supporting Information, pp S4−S5).[39,50] The two thermodynamic cycles in Figure 1 can be used to relate $\Delta_{RS\text{-}S}\Delta G_{sol}$, and hence the eutectic composition (eq 3), to either the difference in free energies of melting, $\Delta_{RS\text{-}S}\Delta G_{melt}$, or the difference in free energy of sublimation, $\Delta_{RS\text{-}S}\Delta G_{subl}$. Focusing on the sublimation cycle we get a relation between α and the sublimation thermodynamics (Figure 1, eq 1) by

$$\alpha = \frac{x_{RS}}{x_S} \approx \exp\left(-2\frac{\Delta_{RS-S}\Delta G_{subl}}{RT}\right) \approx \exp\left(-2\frac{\Delta_{RS-S}\Delta H_{subl}}{RT}\right) \approx \exp\left(2\frac{\Delta_{RS-S}\Delta E_{latt}}{RT}\right) \quad (4)$$

In eq 4 several levels of approximations are implicit which minimize the computational effort to calculate relative solubilities: (i) the solutions of enantiomer and racemate are ideal, or so similar that $\Delta_{RS\text{-}S}\Delta G_{solv} = 0$, and the solvent is achiral; (ii) entropy contributions are the same for the enantiomer and the racemic compound in the solid phase and the gas; (iii) the thermal correction, H_{corr}, (eq 2) is equal for the enantiomer and the racemic compound or even molecule independent, as in the frequently used "$2RT$ approximation":

$$\Delta H_{subl}(T) = -E_{latt} - 2RT \quad (5)$$

This approximation is frequently invoked in the computational prediction of solubilities[51] and sublimation enthalpies of organic molecules.[20] It arises from the equipartition theorem of internal degrees of freedom for the gas and the crystal, assuming an ideal gas and the Dulong-Petit model of a perfect atomic crystal.[52] This relationship enables sublimation enthalpies to be estimated without the need to calculate the vibrational (phonon) modes of the crystal. However, recently this approximation has been shown to be poor, with errors up to 5 kJ mol^{-1} (Supporting Information, Figure S3) for small molecular crystals.[53−55] However, for comparing the thermodynamic *differences* between enantiopure and racemic crystals, parts of the thermodynamic quantities of H_{corr} are likely to cancel out, with the gas phase contributions to H_{corr} (eq 2) being assumed to be identical for both chiral species.

2.2. Lattice and Zero-Point Energies, Heat Capacities, and Entropic Contributions. The lattice energy E_{latt} characterizes a static perfect infinite crystal and an ideal gas phase in its lowest energy conformation, both at 0 K. Taking this as the zero of energy, we can calculate the lattice energy from periodic electronic structure models, $\psi_{crys.}$ Less computationally expensive ψ_{mol} calculations further separate the lattice energy into crystal and isolated molecule contributions, providing a separated model:[56]

$$E_{latt} = U_{inter} + \Delta E_{intra} \quad (6)$$

where ΔE_{intra} is the difference in energy for a single molecule in the crystal conformation and in its lowest energy conformation ($\Delta E_{intra} = 0$ for rigid molecules) and is typically less than a few kJ·mol^{-1} unless intramolecular hydrogen bonding is involved.[44] Both ψ_{crys} and ψ_{mol} models can be used to calculate the lattice vibrations (phonons) from the second derivatives of the lattice energy, i.e., within the harmonic approximation. In the ψ_{mol} model, it is assumed that the molecular modes are unaffected by crystal packing and thus can be estimated from the vibrational frequencies of the isolated molecule and combined with the rigid-body lattice modes. Our ψ_{mol} model is further simplified by only using the $\boldsymbol{k} = 0$ modes of the unit cell, ignoring the difference in size and shape between the racemic and enantiopure crystals. ψ_{crys} generates all the vibrational modes, including the high frequency molecular modes, and calculates the heat capacity, zero-point energies and entropy by integration over the Brillouin zone.[45,57,58] Full details of both computational models are given in Supporting Information, pp S4−S5. Both methods give E_{ZPE} and heat capacities at constant volume C_V. The isobaric and isochoric solid state heat capacities C_P^s and C_V^s are related by the bulk modulus, K, and the thermal volume expansion coefficient α_T.

$$C_P^s(T) = C_V^s(T) + TVK\alpha_T^2 \quad (7)$$

If the thermal expansion of the unit cell is neglected, which is consistent with making the harmonic approximation, we can directly compare experimental $C_P^s(T)$ with computed $C_V^s(T)$. This approximation is made throughout the paper, but it is tested for naproxen using quasi-harmonic calculations (see Supporting Information, p S29−S32).

3. MATERIALS AND METHODS

3.1. Enantiopure and Racemic Compounds and Crystal Forms. Samples of (*S*)-lactide, (*RS*)-lactide, (*S*)-naproxen, (*RS*)-naproxen, (*R*)-3ClMA, (*R,S*)-3ClMA, and (*R*)- and (*RS*)-mandelic acid were available commercially and purified and recrystallized where needed, and confirmed to correspond to single polymorphs (see Supporting Information, p S10 for more information).

3.2. Experimental Methods. *Heat Capacity Measurements.* Low-temperature heat capacities for enantiopure and racemic naproxen and 3ClMA crystals were measured by means of direct heat pulse calorimetry (DHPC) from 2 to 200 K. A commercially

DOI: 10.1021/acs.cgd.7b00582
Cryst. Growth Des. 2017, 17, 4676−4686

available relaxation calorimeter has been used at the Institute of theoretical Physics of the Goethe University in Frankfurt, the physical property measurement system (PPMS) from Quantum Design. Heat capacities above room temperature were measured using a DSC 111 calorimeter from Setaram.[59] Sapphire and benzoic acid were used as reference standards. Average deviations to published data were 1.4% for sapphire[60] and 2.6% for benzoic acid.[61] Additional differential scanning calorimetry (DSC) measurements of the closely related (*R*)- and (*RS*)-mandelic acid molecules were performed between 298 and 370 K using the same measurement method as for the other molecules (more details can be found in the Supporting Information, p S26).

Solid State Raman Spectra. Solid-state Raman analysis of the powdered crystals was performed with a commercial MultiRAM spectrometer from Bruker, Germany. The system employs a laser beam at 1064 nm and was operated at 500 mW. The analyses were carried at ambient temperature averaging over 32 scans with a spectral resolution of 1 cm^{-1} between 10 and 3500 cm^{-1}.

Eutectic Composition and Thermochemical Properties. Eutectic compositions in various solvent systems were taken from literature for lactide[62,63] and 3ClMA.[30,63] and measured here for (*S*)- and (*RS*)-naproxen (see Supporting Information, Table 28). Additional solubilities were measured in a variety of solvents for lactide to supplement previous measurements. Melting properties, vapor pressures, and corresponding enthalpies and free energies of sublimation were taken from the literature[27,30,64,65] where available and are summarized in the Supporting Information, Tables S3–S4.

3.3. Computational Methods. Within the electronic (ψ_{crys}) model we compare thermochemical properties from two approximate dispersion corrected periodic electronic structure methods based on a minimal basis set Hartree–Fock (HF-3c)[66,67] and on a tight-binding Hamiltonian (DFTB3-D3).[53] HF-3c and DFTB3 calculations were performed with a developer version of CRYSTAL14,[68] and DFTB+,[69] respectively. In the separated ψ_{mol} model, the isolated molecular structures were geometry optimized and molecular vibrations in the rigid rotor harmonic oscillator (RRHO) approximation were calculated at the PBE/def2-TZVP level of theory using the D3 dispersion correction[70] with TURBOMOLE V6.4.[71] The rigid-molecule lattice frequencies were calculated using DMACRYS.[56] The lattice energy was determined using CrystalOptimizer[72] allowing the flexible torsion angles in Figure 2 to adapt to the packing forces. In order to compare experimental and computational enthalpic and entropic contributions, a combined "exp/theory" method is constructed, in which experimental heat capacities are interpolated and numerically integrated using spline functions within MATLAB (Mathworks). These can be combined with calculated ideal gas heat capacities from the isolated molecular frequencies and calculated zero-point energies from ψ_{mol} to give H_{corr} and sublimation entropies according to eq 2. The free energy of solvation, ΔG_{solv}, was computed with the thermodynamic model COSMO-RS[73] including the distinct flexibility of the three molecules by a Boltzmann weighting of possible conformers. For more details see Supporting Information, pp S35–S36.

4. RESULTS

4.1. Temperature-Dependent Solid State Heat Capacities. Temperature-dependent heat capacity measurements for enantiopure and racemic crystalline powders of the three substances were recorded in temperature ranges from 2 to 202 K and 298 to 410 K (or until melting) and are given in the Supporting Information, Figures S4–S5, and tabulated in comparison with the calculated values (Supporting Information, Tables S13–S22). At very low temperatures the heat capacities follow Debye's cubic law ($C_P \propto T^3$), then increase linearly with temperature and do not level even approaching the highest temperatures of 400 K. Thus, the assumption of mode saturation in the 2*RT* correction (eq 3) is not valid for any of the organic molecular crystals. Naproxen has a significantly larger heat capacity than 3ClMA and lactide due to the larger number of atoms per molecule. The results are in agreement with previous measurements for the lactide[64,74] and naproxen[75] and within the 1–5% accuracy of DSC[76] heat capacity measurements. The calculated temperature-dependent heat capacities reproduce the temperature dependence up to 200 K and also give the differences in magnitude between the different organic molecules. At higher temperature, the calculations appear to systematically underestimate heat capacities. which was also found for many small molecular crystals.[48] A systematic experimental overestimate of high temperature DSC could be ruled out by comparing to benzoic acid and sapphire (see Supporting Information, p S12 and S28 for more information).

4.2. Heat Capacity Differences between Enantiomeric and Racemic Crystals. Since we are focusing on the free energy differences and relative thermodynamic quantities, heat capacity differences between the racemic and enantiopure substances, $\Delta_{RS-S}C_P(T) = C_{P,RS} - C_{P,S}$, are discussed. Below 100 K, the experimental heat capacity differences are between −1 and 3 J mol^{-1} K^{-1} and distinguishable between the three molecules (Figure 3), changing in sign between molecules and

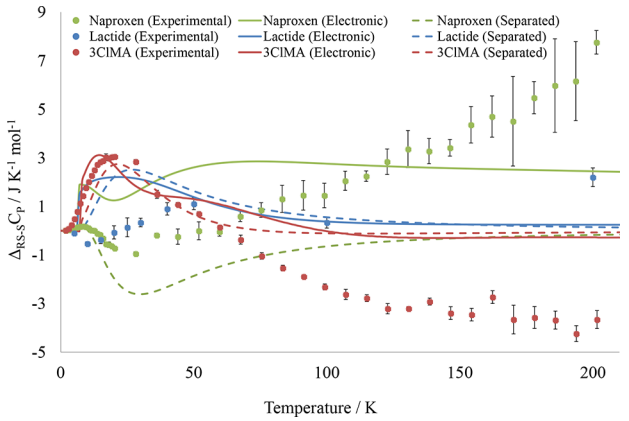

Figure 3. Low temperature heat capacity differences, $\Delta_{RS-S}C_P$, between racemic and enantiopure crystals. Experimental results (dots) are shown with experimental uncertainty and compared with calculated $\Delta_{RS-S}C_V$ values from electronic ψ_{crys} HF-3c (solid lines) and separated ψ_{mol} (dashed lines) phonon modes.

with temperature. The naproxen heat capacity difference for example changes sign twice, rising between 150 and 200 K. The heat capacities for naproxen above 150 K have significant experimental error bars due to a loss in thermal coupling as described by the supplier.[77] The calculated heat capacities from ψ_{crys} only qualitatively reproduce differences between enantiomer and racemate at the low temperatures, but do show a marked system dependence. The computed harmonic rigid-molecule, mode separated ψ_{mol} calculations in Figure 3 show an asymptotic approach to heat capacity differences of zero for all compounds.

The heat capacity differences between the racemic and enantiopure substances, $\Delta_{RS-S}C_P(T)$, at 298 K are summarized in Table S25 in the Supporting Information. The high temperature heat capacity differences in the range of 300–370 K in Figure 4 are particularly pronounced for 3ClMA, where the heat capacity of the enantiomer at 298 K is 211.1 ± 1.6 J mol^{-1} K^{-1}, which is 9.2 ± 2.2 J mol^{-1} K^{-1} (4.5%) larger than that of the racemic crystal (201.9 ± 1.5 J mol^{-1} K^{-1}; see Figure 4). Such a significant heat capacity difference had

DOI: 10.1021/acs.cgd.7b00582
Cryst. Growth Des. 2017, 17, 4676–4686

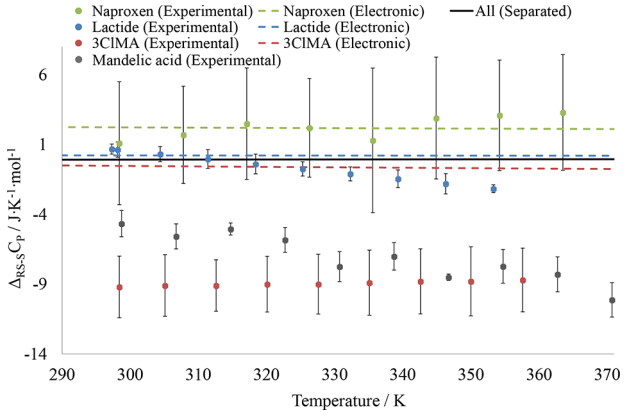

Figure 4. Experimental high temperature heat capacity differences, $\Delta_{RS\text{-}S}C_P$, between the racemate and the enantiomer. Computed electronic ψ_{crys} HF-3c $\Delta_{RS\text{-}S}C_V$ are given as dashed lines in the same color; separated ψ_{mol} $\Delta_{RS\text{-}S}C_V$ are zero (black straight line).

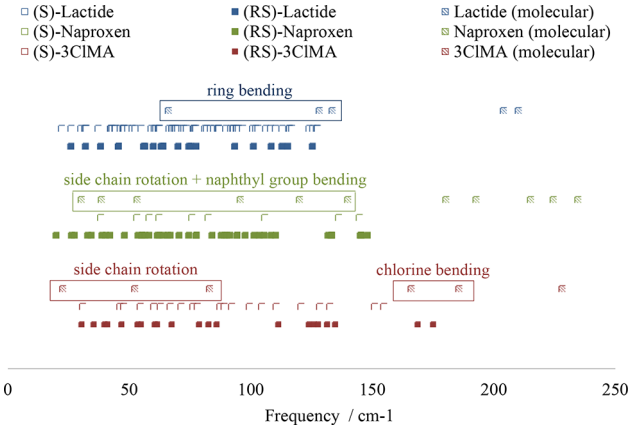

Figure 5. Comparison of the rigid-molecule $k = 0$ lattice frequencies of the enantiopure and racemic crystals of lactide, 3ClMA, and naproxen with their isolated molecule low frequency modes, to assess the validity of the separation model ψ_{mol}. Numerical values are in the Supporting Information (Tables S5–S10).

previously been reported for mandelic acid[31] at temperatures that are relevant for a crystallization process (5–70 °C), so we repeated the experiment for (*RS*)- and (*S*)-mandelic acid (see Supporting Information, S23–S24 for primary data) to confirm the previous results,[31] and found that the heat capacity difference between the enantiopure and racemic crystals increases with temperature for mandelic acid but is almost constant for 3ClMA (Figure 4). At 298 K the lactide shows a small heat capacity difference, with that of the (*RS*)-lactide being only 0.6 ± 0.5 J·mol^{-1} K^{-1} larger than that of the enantiomer, though this value is smaller than a previously published value of 2.8 ± 0.3 J·mol^{-1} K^{-1}.[64,74] The heat capacity differences of naproxen at room temperature are 1.3 ± 4.9 J·mol^{-1} K^{-1} and within experimental uncertainty. The periodic electronic structure calculations do show a small difference in the heat capacities at process-relevant temperatures for naproxen but this is independent of temperature. The separated model ψ_{mol} gives no heat capacity differences at elevated temperatures for any molecule. This requires a thorough investigation of the assumptions behind current theoretical models.

4.3. Analysis of Molecular and Lattice Vibrations from Theoretical Models and Underlying Assumptions. Integration of lattice vibrational modes (Supporting Information, Tables S8–S10) yields the heat capacities, characteristic for both molecule type and crystal packing. The separated Ψ_{mol} model assumes the lattice modes to be sufficiently separated in energy and uncoupled from molecular vibrational modes (see Supporting Information, Tables S5–S7). Hence, the separated model ψ_{mol} inevitably predicts that $\Delta_{RS\text{-}S}C_P$ tends to zero with increasing temperature at about 150 K, well below ambient temperatures (Figure 3) as the molecular modes are assumed to be unaffected by the crystal structure. This does not hold for any of the compounds (see Figure 5). Even for the "rigid" lactide, there are some ring bending modes that are of similar frequencies to the lattice modes. For naproxen, the low frequency molecular modes are rotations of the propionic acid side chain and bending of the naphthyl ring, which is nonplanar in the enantiopure crystal structure.[78] The low frequency molecular modes of 3ClMA are rotations of the flexible alpha-hydroxy acid side chain and out-of-plane vibrations of the chlorine atom. These very low frequency molecular modes may couple with certain lattice modes and affect the heat capacities at low temperatures (see equations in Supporting Information, S9–S11).

All three molecules pack so differently in the racemic and enantiopure structures that the lowest frequency modes are very different in nature.

Figure 6 shows the packing differences and the lowest energy lattice modes within the unit cells. (*RS*)-naproxen has a layered structure, with only weak van-der-Waals forces between the

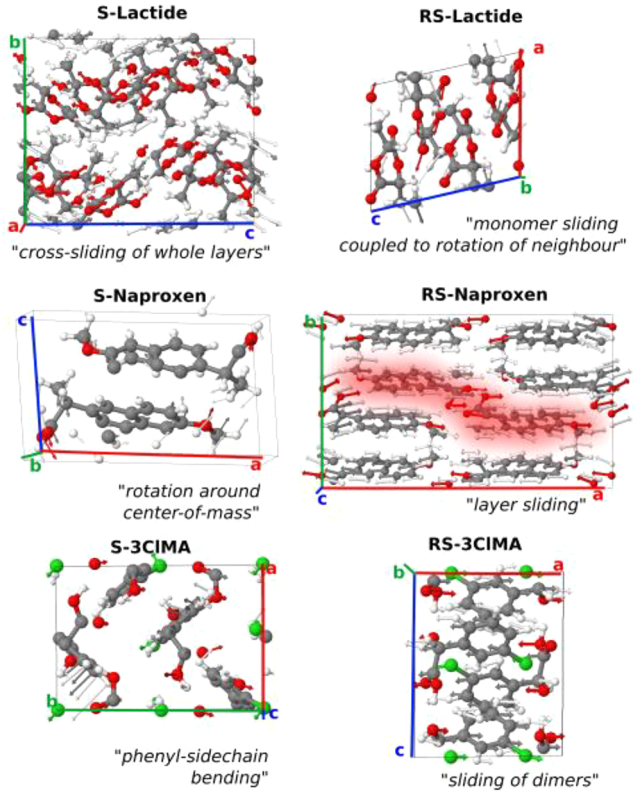

Figure 6. Packing of the crystals showing the lowest energy lattice modes by vectors in atomic colors representing the amplitude and direction of the vibrations from HF-3c $k = 0$ electronic structure calculations. The red shading shows the hydrogen-bonded naproxen layer.

DOI: 10.1021/acs.cgd.7b00582
Cryst. Growth Des. 2017, 17, 4676–4686

zigzag layers of hydrogen bonded dimers. The lowest frequency lattice mode corresponds to a relative sliding of the layers with respect to each other. In (*S*)-naproxen, there are hydrogen-bonded chains which rotate relative to each other. In (*RS*)-3ClMA, pairs of hydrogen-bonding layers slide relative to each other, whereas in (*S*)-3ClMA the lowest mode is predominately that of flexible torsion around Φ_1 (Figure 6).

The actual frequencies of these modes will be very sensitive to the choice of computational method and its potential energy surface; indeed, the less computationally demanding periodic electronic structure DFTB3-D3 yields significant differences in low temperature heat capacities compared with the HF-3c calculations (Supporting Information, Tables S11−S22 and Figures S4−S5). Comparable errors result from the assumption that the molecule is rigid and the use of an atom−atom intermolecular potential energy surface in the separated ψ_{mol} model for flexible molecules such as naproxen and 3ClMA.

The results of ψ_{mol} and ψ_{crys} are more consistent for the more rigid lactide, which has more isotropic and very weak intermolecular interactions and shows smaller heat capacity differences. Hence, ψ_{mol} and ψ_{crys} both fail in quantitatively calculating the low-temperature heat capacity differences and only give qualitative agreement with experiment (Figure 3) for the molecules that are more typical of pharmaceuticals. However, the error introduced by neglecting the coupling of molecular and lattice vibrational modes and using different computational models is very dependent on the molecule and crystal structure.

For the high temperature heat capacities, only the high frequency molecular modes are relevant, as the low frequency lattice modes have become saturated. The electronic ψ_{crys} calculations give differences in the high frequency modes that lead to a small difference in heat capacities at process-relevant temperatures for naproxen and 3ClMA but not for the lactide (Figure 4). The electronic calculations, however, systematically underestimate the high temperature heat capacities (Supporting Information, Figure S11−S22) which contributes to the poor predictions of the heat capacity differences (Figure 4). Differences in molecular and lattice vibrations can be obtained from the solid-state Raman spectra[79] for the enantiopure and racemic crystals (see Figure 7). For naproxen and 3ClMA, there are detectable differences between the crystal forms in particular at higher frequencies, i.e., the C═O around 1600−1800 cm^{-1} and O−H around 3000 cm^{-1}. For lactide, enantiopure and racemic crystals display an almost identical Raman spectrum (Figure 7). Differences in the higher frequency molecular modes between the racemic and enantiopure crystals are necessary and a strong pointer for a difference in the heat capacities at process-relevant temperatures.

The harmonic approximation is made in all the calculations and is likely to be poor at relevant temperatures for most organic crystals, as this is relatively close to their melting points (Supporting Information, Table S3). The harmonic approximation completely neglects thermal expansion of crystals, which can differ markedly in its anisotropy with the differences in molecular packing. The anisotropic expansion of naproxen has been estimated by a quasi-harmonic approximation (Supporting Information, pp 29−32) and leads to an increase in the room temperature C_P (by 7 and 8 J mol^{-1} K^{-1} for *RS* and *S* respectively) relative to the harmonic underestimate. Using a fully anharmonic model from Molecular Dynamics trajectories

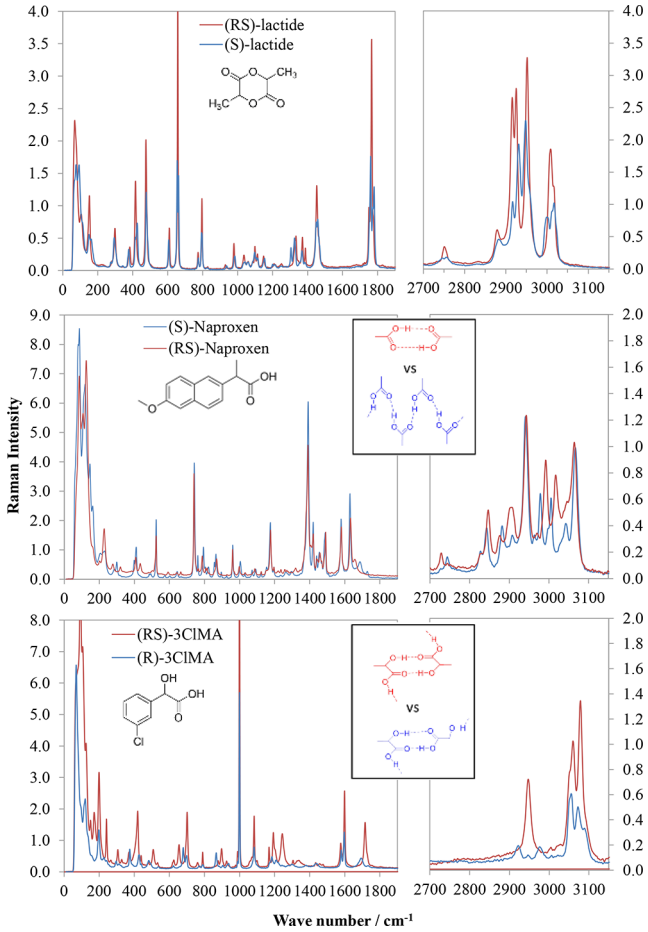

Figure 7. Solid-state Raman spectra of the racemic and enantiopure crystals between 0 and 1800 cm^{-1} and 2700−3150 cm^{-1}. The inset illustrates the different hydrogen bonding motifs, responsible for the changes in the spectra at higher frequencies, i.e., the C═O around 1600−1800 cm^{-1} and O−H around 3000 cm^{-1}.

for heat capacities would be expected to further improve the agreement with experiment.

4.4. Comparing Thermochemical Properties for Enantiopure and Racemic Crystals from Experiment and Theory. Figure 8 shows the sublimation enthalpies as estimated using the experimental and calculated thermochemical properties (values in Supporting Information, Table S26). The lattice energy is the major contribution to the absolute values of the enthalpies of sublimation and the differences between the racemate and enantiomer when compared to the experimental values, where available (Figure 8). However, the heat capacity and zero-point energy terms are still significant and cannot be neglected in any computational estimates of the sublimation enthalpy.

There is a clear correlation between the differences in the thermal corrections with the flexibility and packing in racemic and enantiopure crystal structures. The molecule and crystal-specific phonon frequencies affect the thermal corrections H_{corr} (eq 2), and the "2RT-approximation" is as inadequate for these organic crystals as it is for those comprised of smaller molecules (see Supporting Information, Figure S3).

For the lactide species, thermal corrections from separated and periodic calculations are very close and the (*RS*-*S*) differences are in excellent agreement with experimental heat capacities corrections, although there are errors in the absolute

DOI: 10.1021/acs.cgd.7b00582
Cryst. Growth Des. 2017, 17, 4676−4686

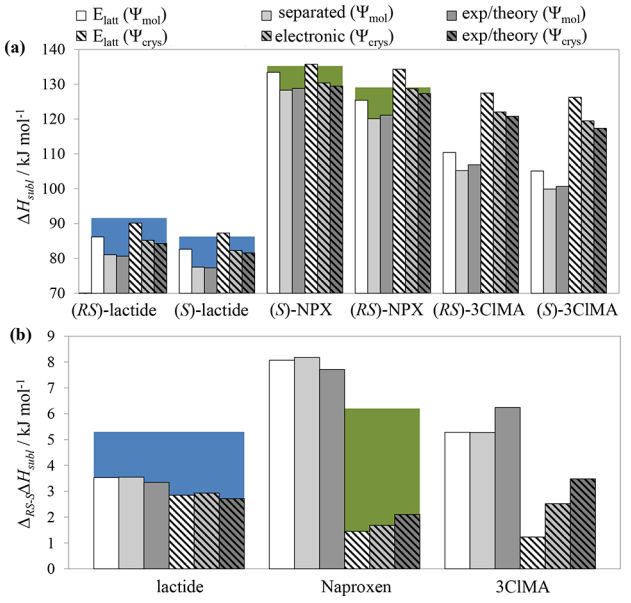

Figure 8. (a) Absolute sublimation enthalpies, ΔH_{subl}, and (b) sublimation enthalpy differences between the racemate and enantiomer, $\Delta_{RS\text{-}S}\Delta H_{subl}$, compared to experiment as colored background: (blue = lactide;[65] green = naproxen;[27] 3ClMA decomposes), with the plain bars corresponding to the separated model and the striped to the electronic model.

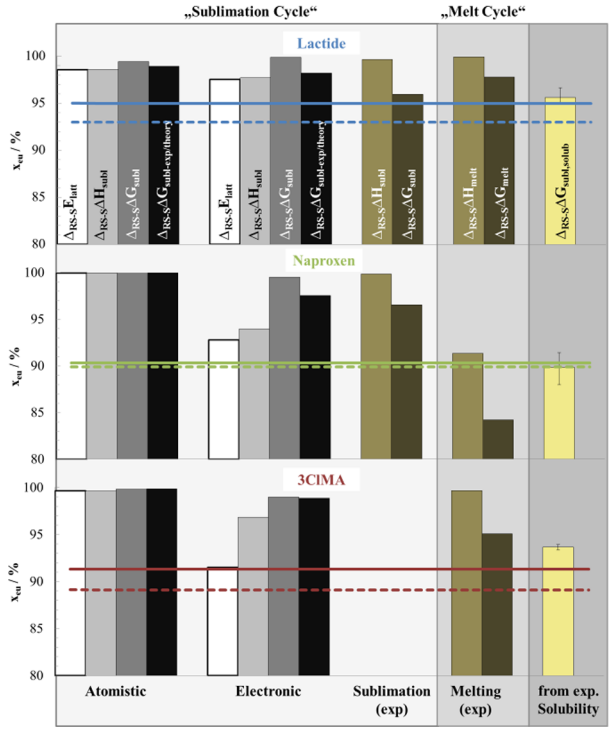

Figure 9. Eutectic compositions at 298 K. Calculated lattice energy, enthalpy corrections, and entropy differences (white, light gray, and gray) from ψ_{mol} and ψ_{crys} in the sublimation cycle compared with experiments from both cycles (green) and measured solubilities (yellow) in different solvents. The error bar is its variation. Maximum (solid line) and minimum (dashed line) values of x_{eu} in various solvents at 298 K are also given.

C^s_P (see Supporting Information, Figure S4). However, for naproxen and 3ClMA the different hydrogen bonding in the two crystals and increasing vibrational flexibility lead to larger differences in thermal corrections. The effect of including the coupling between the molecular and lattice modes is relatively small. The magnitude, however, is still comparable to the neglect of thermal expansion of the unit cell, which is estimated for naproxen (Supporting Information, Figure S9) to lead to an error of about 1 kJ mol^{-1} in H_{corr}. The differences between the calculated and experimental heat capacities are a significant source of error in ΔH_{subl}, up to 2.2 kJ mol^{-1} for (*S*)-3ClMA (Supporting Information, Table S27).

4.5. Estimating the Eutectic Composition and Its Temperature and Solvent Dependence. The eutectic composition is the key parameter for chiral separation. It can depend on temperature, the nature of the solvent, or both. Figure 9 compares calculations of x_{eu} from the thermodynamic cycle using $\Delta_{RS\text{-}S}\Delta G_{subl}$, assuming that x_{eu} is independent of solvent, with experimental data at 298 K.

A comparison is also made with alternative methods of estimating the eutectic composition. Experimentally, x_{eu} can, in principle, be estimated using the “sublimation cycle” or the “melt cycle” (Figure 1). In the latter, the solution free energy is obtained via the supercooled melt (ΔG_{melt}) by using experimental differences in free energies of melting $\Delta_{RS\text{-}S}\Delta G_{melt}$ (Supporting Information, Tables S3 and S29). The melt cycle assumes that the free energy of mixing with the solvent (ΔG^E) is the same for both racemic and enantiopure crystals. Thus, the melt cycle is making the same assumption as the sublimation cycle, that the solution nonidealities of both chiral species are the same ($\Delta_{RS\text{-}S}\Delta G^E = 0$). Results for x_{eu} from the melt cycle are comparable to the sublimation cycle for lactide only. For naproxen, where both the racemic and enantiopure crystals have almost the same melting temperature and enthalpies, the melt cycle significantly underestimates the Gibbs energy difference and hence the eutectic composition.

An alternative approach to estimating x_{eu}, concentrates on the solvent, and uses experimentally measured solubilities of enantiomer and racemate in a variety of solvents (Supporting Information, Table S28) to obtain ΔG_{sol}. If the molecular solvation free energies are calculated using COSMO-RS[73] at infinite dilution, and assuming ideal solutions, then $\Delta G_{subl,solub}$, can be recursively calculated via the sublimation cycle from solubilities (see Supporting Information, Table S29).

A cross check on this procedure is that the estimates of $\Delta_{RS\text{-}S}\Delta G_{subl,solub}$ are in good agreement with the free energies from available vapor pressure measurements (Supporting Information, Table S29) differing only by 0.1 kJ mol^{-1} for lactide and 1.4 kJ mol^{-1} for naproxen. Experimental solubilities to estimate x_{eu} (Figure 9 yellow bar) give a variation with solvent which is of the same order of magnitude as the variation of x_{eu} in different solvents at 298 K for lactide, while it is overestimated for naproxen and underestimated for 3ClMA.

This shows that there is a significant solvent effect on the eutectic composition at a given temperature because the solutions of the three molecules involved are not ideal, and that this nonideality differs between the racemic and enantiopure solutions.

The accuracy of computational predictions of x_{eu} via the sublimation cycle is critically dependent on the accuracy of lattice energy differences. They systematically overestimate the eutectic compositions, as previously found for amino acids in water.[39] The enthalpy correction, ΔH_{corr}, only contributes significantly to x_{eu} in the case of 3ClMA, but entropic

DOI: 10.1021/acs.cgd.7b00582
Cryst. Growth Des. 2017, 17, 4676−4686

differences account for up to 4 kJ·mol^{-1} to $\Delta_{RS\text{-}S}\Delta G_{\mathrm{subl}}$ and thus affect x_{eu} for all molecules. Direct use of the sublimation cycle when sublimation data are available gives very similar estimates of x_{eu} (Figure 9). The combination of electronic structure calculations and experimental solubilities "exp/theory" (black bar in Figure 9) to yield $\Delta_{RS\text{-}S}\Delta G_{\mathrm{subl,exp/theory}}$, gives the best estimate of x_{eu} and correlates well with experimental sublimation free energies[27,65] when using the ψ_{crys} model.

The observed temperature dependence of x_{eu} (Supporting Information, Table S28) cannot be accounted for by the calculations, but can be estimated by numerically integrating the measured heat capacity differences between 298 and 318 K. There is a small temperature effect on the Gibbs free energy of sublimation differences $\Delta^{\mathrm{T1\text{-}T2}}\Delta_{RS\text{-}S}\Delta G_{\mathrm{subl}}$ which slightly shifts the eutectic composition: for lactide and naproxen, x_{eu} decreases by −0.4 and −0.9 mol % and increases by 0.6 mol % for 3ClMA. In the experiment, these values are dependent on solvent and vary between 0 and −3.0 for lactide and 0 and 1.3 for 3ClMA. For naproxen, the solvent independent shift is slightly underestimated (−1.2 mol %). Thus, the nature of the solvent not only affects the eutectic composition at a given temperature but may also promote or prevent shifts of x_{eu} with temperature. There are examples in the literature, where x_{eu} is temperature dependent in one solvent and independent in another.[7] Unlike 3ClMA, the eutectic composition of mandelic acid is constant at x_{eu} = 69% and shows no variation in different solvents and over a large temperature range.[4] This is surprising as mandelic acid displays a difference in heat capacity between the racemic and enantiopure crystal which is dependent on temperature.[31] This has to be explained by a cancellation of different effects. We have to conclude that the eutectic composition and its temperature dependence $\Delta x_{\mathrm{eu}}(T)$ is not a mere solid state property. Accurate predictions will have to consider the differences in solvation free energies for the racemic and enantiopure solutions. This implies consideration of the nonideality of the solution in terms of the specific molecule, its solvent, as well as solute−solute interactions.

5. DISCUSSION

5.1. Differences in Gibbs Free Energies from Thermodynamic Cycles. Two thermodynamic cycles, the "melt" and the "sublimation" cycle enable the eutectic shift x_{eu} to be estimated from the thermodynamic properties of the enantiopure and racemic compound. We have shown that the sublimation cycle is competitive in accuracy with the traditional melt cycle and has the advantage that the required solid-state thermodynamic quantities can, in principle, be estimated computationally with high accuracy.[80] However, our detailed comparison for three diverse systems shows that there is a strong dependence of the thermochemical properties on the intermolecular interactions and molecular flexibility differences in the racemic and enantiopure crystals. Heat capacity differences at ambient temperature for the enantiopure and racemic forms of pharmaceuticals could provide a sufficient temperature-dependent shift in the eutectic composition to enable a resolution of enantiomers by a two-step crystallization process. A necessary requirement for this is a difference in the high frequency molecular vibrational modes between the two crystals, which should be apparent in the Raman or infrared spectrum, and is likely to be linked to changes in hydrogen bonding interactions. Many other assumptions frequently used when modeling organic solid state thermodynamics do not hold. Phonon modes, which are dependent on crystal packing, lead to thermal expansion at finite temperature and solid state heat capacities which may differ between the racemic and enantiopure crystals. The often made assumption that lattice energies and sublimation enthalpies differ by 2RT, so that the molecular motion in crystals can be neglected, is over-simplifying the thermodynamics of industrially important organic crystals. Our results also confirm that assuming the solvation energy is the same for the enantiopure and racemic compound is not always realistic enough for the prediction of eutectic shifts.[81]

5.2. Computational Challenges. The separation of enantiomers poses a challenge to modern computational methods. When lattice energy calculations show that the racemic crystal is much more stable than the enantiopure, the enantiomers in the racemate cannot be separated, but a simple thermodynamically controlled one-step crystallization will remove the racemate leaving an enantiopure solution.[21] In the case of small lattice energy differences, separation of enantiomers by a two-step crystallization process may be exploitable. It is very rare for the molecular chirality to provide a strong preference for a chiral packing in all three directions, such that an enantiopure crystal is significantly more stable than any racemic structure.[82]

Current state-of-the-art electronic structure methods typically have lattice energy errors in the range of 3−7 kJ·mol^{-1} for crystals of small organic molecules.[83,84] When lattice energy differences are small enough for chiral separation to be feasible, <4 kJ·mol^{-1}, the differences in thermodynamic contributions that arise from the finite temperature effects become significant. The degree of cancellation between zero-point lattice energy, thermal corrections, and entropy terms will depend on the specific crystal structures. When the molecule is rigid and the intermolecular interactions are not affecting the molecular structure or vibrations, there is only a difference in heat capacities at low temperatures. However, for flexible molecules, particularly if there is a difference in the hydrogen bonding and anisotropy of thermal expansion, relative heat capacities at ambient temperatures will require periodic electronic structure calculations of lattice and molecular vibrations plus inclusion of thermal expansion effects. When accurate harmonic modes can be calculated, these are likely to underestimate heat capacities at process relevant temperatures because of the neglect of thermal expansion. Even the quasi-harmonic approximation may not be adequate for absolute heat capacities, as shown by a comparison of phonon modes by lattice and molecular dynamics.[85] Flexible pharmaceuticals can have very anharmonic intramolecular modes, such as methyl rotations and large amplitude phenyl librations. While there is a clear path to improving the calculation of the solid-state thermodynamics in the sublimation cycle, it is less clear how the observed effects of the solvent on the eutectic shift can be predicted without explicit solvent molecular dynamics as nonidealities of mixtures need to be considered. Thus, a reliable computational prediction of the eutectic shift and its dependence on temperature and solvent will require great accuracy in all contributions to the thermodynamic cycles.[86]

5.3. Indications of Eutectic Shifts. Resolution of enantiomers by selective crystallization can be supported by theoretical approaches. High quality calculated lattice energy differences can determine when crystal energies are too large for a separation by crystallization to be possible. Phonon calculations can show whether the differences in crystal structures results are likely to lead to significant heat capacity

DOI: 10.1021/acs.cgd.7b00582
Cryst. Growth Des. 2017, 17, 4676−4686

differences. A difference in the higher frequency "molecular modes" in the Raman spectra of the two crystals is a strong indicator of a shift in eutectic composition exploitable in a process-relevant temperature range. The fundamental experimental choice of solvent could be assisted by looking for changes in the free energies of sublimation derived from experimental solubilities correcting for the computed molecular solvation energy. This might replace some of the tedious determinations of many ternary phase diagrams. However, the prediction of eutectic shifts may still be limited by the assumption of equilibrium thermodynamic models to describe crystallization, which appears questionable for some systems.[29,87]

6. CONCLUSION

We have compared computed and experimental thermodynamic data for three pairs of enantiopure and racemic crystals of prototypical organic molecules, which are more representative of pharmaceuticals than crystals composed of atoms or small, rigid molecules. The sublimation cycle offers considerable promise as a method of evaluating the possibilities for chiral resolution by crystallization, which can be done by a combination of calculations and experimental data. Some systematic errors in both experimental procedures and theoretical assumptions have widely been expected to cancel in the differences between enantiopure and racemic crystals, or in estimating derived thermodynamic quantities. However, the degree of cancellation has been shown to be very dependent on the molecule, its functional groups, and their flexibility and how this is manifested in differences in the solid-state structures and solution behavior. Reliably predicting the eutectic composition is still a major challenge to computational modeling and the rational exploitation of crystallization processes. However, molecular-level insights into the differences between specific enantiopure and racemic structures can help assess the feasibility of designing processes to separate enantiomers.

■ ASSOCIATED CONTENT

Supporting Information

The Supporting Information is available free of charge on the ACS Publications website at DOI: 10.1021/acs.cgd.7b00582.

Additional information regarding computational details, materials and methods and experimental measurements of heat capacities and solubilities (PDF)

■ AUTHOR INFORMATION

Corresponding Authors

*(M.S.) E-mail: matthias.stein@mpi.magdeburg.mpg.de.
*(S.L.P.) E-mail: s.l.price@ucl.ac.uk.

ORCID

Andreas Seidel-Morgenstern: 0000-0001-7658-7643
Matthias Stein: 0000-0001-7793-0052
Sarah L. Price: 0000-0002-1230-7427

Author Contributions

#H.B. and R.K.H. contributed equally.

Funding

Max Planck Society for the Advancement of Science, ESPRC EP/K039229/1 and the EU COST Action CM1402.

Notes

The authors declare no competing financial interest.

■ ACKNOWLEDGMENTS

R.K.H. is grateful for a UCL-MPS Impact Ph.D. Fellowship. J.G.B. acknowledges support by the Humboldt foundation within the Feodor-Lynen program. This work was also supported in part by the Max Planck Society for the Advancement of Science, ESPRC EP/K039229/1 and the EU COST Action CM1402 "Crystallize". We thank Prof. K. Refson for discussions and help with preliminary work on DFT-D calculations which were performed on ARCHER, via our membership of the UK's HPC Materials Chemistry Consortium, funded by EPSRC (EP/L000202). Dr. N. van Well and Prof. C. Krellner from the Goethe University Frankfurt are acknowledged for support of the low temperature heat capacity measurements.

■ REFERENCES

(1) Nguyen, L. A.; He, H.; Pham-Huy, C. Chiral Drugs: An Overview. *Int. J. Biomed. Sci.* **2006**, *2* (2), 85−100.
(2) *Development of New Stereoisomeric Drugs*; U.S. Food and Drug Administration, 1992.
(3) Ulrich, E. M.; Morrison, C. N.; Goldsmith, M. R.; Foreman, W. T. Chiral Pesticides: Identification, Description, and Environmental Implications. In *Reviews of Environmental Contamination and Toxicology*; Whitacre, D. D. M., Ed.; Springer: New York, 2012.
(4) Lorenz, H.; Seidel-Morgenstern, A. Processes To Separate Enantiomers. *Angew. Chem., Int. Ed.* **2014**, *53* (5), 1218−1250.
(5) Otero-de-la-Roza, A.; Hein, J. E.; Johnson, E. R. Reevaluating the Stability and Prevalence of Conglomerates: Implications for Preferential Crystallization. *Cryst. Growth Des.* **2016**, *16* (10), 6055−6059.
(6) Klussmann, M.; White, A. J. R.; Armstrong, A.; Blackmond, D. G. Rationalization and prediction of solution enantiomeric excess in ternary phase systems. *Angew. Chem., Int. Ed.* **2006**, *45* (47), 7985−7989.
(7) Lorenz, H.; Le Minh, T.; Kaemmerer, H.; Buchholz, H.; Seidel-Morgenstern, A. Exploitation of shifts of eutectic compositions in crystallization-based enantioseparation. *Chem. Eng. Res. Des.* **2013**, *91* (10), 1890−1902.
(8) Grant, D. J. W.; Higuchi, T. *Solubility Behavior of Organic Compounds*; John Wiley and Sons: New York, 1990.
(9) Palmer, D. S.; Llinàs, A.; Morao, I.; Day, G. M.; Goodman, J. M.; Glen, R. C.; Mitchell, J. B. O. Predicting Intrinsic Aqueous Solubility by a Thermodynamic Cycle. *Mol. Pharmaceutics* **2008**, *5* (2), 266−279.
(10) Chu, K. A.; Yalkowsky, S. H. Predicting Aqueous Solubility: The Role of Crystallinity. *Curr. Drug Metab.* **2009**, *10* (10), 1184−1191.
(11) Yalkowsky, S. H.; Wu, M. Estimation of the Ideal Solubility (Crystal-Liquid Fugacity Ratio) of Organic Compounds. *J. Pharm. Sci.* **2010**, *99* (3), 1100−1106.
(12) Ran, Y. Q.; Jain, N.; Yalkowsky, S. H. Prediction of aqueous solubility of organic compounds by the general solubility equation (GSE). *J. Chem. Inf Comp Sci.* **2001**, *41* (5), 1208−1217.
(13) Hughes, L. D.; Palmer, D. S.; Nigsch, F.; Mitchell, J. B. O. Why Are Some Properties More Difficult To Predict than Others? A Study of QSPR Models of Solubility, Melting Point, and Log P. *J. Chem. Inf. Model.* **2008**, *48* (1), 220−232.
(14) Diedrichs, A.; Gmehling, J. Solubility Calculation of Active Pharmaceutical Ingredients in Alkanes, Alcohols, Water and their Mixtures Using Various Activity Coefficient Models. *Ind. Eng. Chem. Res.* **2011**, *50* (3), 1757−1769.
(15) Tetko, I. V.; Sushko, Y.; Novotarskyi, S.; Patiny, L.; Kondratov, I.; Petrenko, A. E.; Charochkina, L.; Asiri, A. M. How Accurately Can We Predict the Melting Points of Drug-like Compounds? *J. Chem. Inf. Model.* **2014**, *54* (12), 3320−3329.
(16) Gharagheizi, F.; Gohar, M. R. S.; Vayeghan, M. G. A quantitative structure−property relationship for determination of enthalpy of fusion of pure compounds. *J. Therm. Anal. Calorim.* **2012**, *109* (1), 501−506.

DOI: 10.1021/acs.cgd.7b00582
Cryst. Growth Des. 2017, 17, 4676−4686

(17) Klamt, A.; Eckert, F.; Hornig, M.; Beck, M. E.; Bürger, T. Prediction of aqueous solubility of drugs and pesticides with COSMO-RS. *J. Comput. Chem.* **2002**, *23* (2), 275−281.
(18) Ruether, F.; Sadowski, G. Modeling the Solubility of Pharmaceuticals in Pure Solvents and Solvent Mixtures for Drug Process Design. *J. Pharm. Sci.* **2009**, *98* (11), 4205−4215.
(19) McDonagh, J. L.; Nath, N.; De Ferrari, L.; van Mourik, T.; Mitchell, J. B. O. Uniting Cheminformatics and Chemical Theory To Predict the Intrinsic Aqueous Solubility of Crystalline Druglike Molecules. *J. Chem. Inf. Model.* **2014**, *54* (3), 844−856.
(20) McDonagh, J. L.; Palmer, D. S.; Mourik, T. v.; Mitchell, J. B. O. Are the Sublimation Thermodynamics of Organic Molecules Predictable? *J. Chem. Inf. Model.* **2016**, *56* (11), 2162−2179.
(21) Jaques, J.; Collet, A.; Wilen, S. *Enantiomers, Racemates, and Resolutions*; Wiley and Sons Inc.: New York, 1981.
(22) Toda, F. *Enantiomer Separation: Fundamentals and Practical Methods*; Kluwer Academic, Dordrecht, 2007.
(23) Klimm, D. Phase Equilibria. In *Handbook of Crystal Growth*, 2nd ed.; Nishinaga, T., Ed.; Elsevier: Boston, 2015; Vol. *A*, pp 85−136.
(24) van Hummel, G. J.; Harkema, S.; Kohn, F. E.; Feijen, J. Structure of 3,6-dimethyl-1,4-dioxane-2,5-dione [D-,D-(L-,L-)lactide]. *Acta Crystallogr., Sect. B: Struct. Crystallogr. Cryst. Chem.* **1982**, *38* (5), 1679−1681.
(25) Belen'kaya, B. G.; Bel'skii, V. K.; Dement'ev, A. I.; Sakharova, V. I.; Chernikova, N. Y. Crystal and Molecular Structures of Glycolide and Lactide: Association through CH···O Hydrogen Bonds. *Crystallogr. Rep.* **1997**, *42* (3), 449−452.
(26) Auras, R.; Lim, L.-T.; Selke, S.; Tsuji, H. *Poly(Lactid Acid) − Synthesis, Structures, Properties, Processing and Application*; John Wiley & Sons: Hoboken, NJ, 2010.
(27) Buchholz, H.; Emel'yanenko, V. N.; Lorenz, H.; Verevkin, S. P. An Examination of the Phase Transition Thermodynamics of (S)- and (RS)-Naproxen as a Basis for the Design of Enantioselective Crystallization Processes. *J. Pharm. Sci.* **2016**, *105* (5), 1676−1683.
(28) Braun, D. E.; Ardid-Candel, M.; D'Oria, E.; Karamertzanis, P. G.; Arlin, J. B.; Florence, A. J.; Jones, A. G.; Price, S. L. Racemic Naproxen: A Multidisciplinary Structural and Thermodynamic Comparison with the Enantiopure Form. *Cryst. Growth Des.* **2011**, *11* (12), 5659−5669.
(29) Hylton, R. K.; Tizzard, G. J.; Threlfall, T. L.; Ellis, A. L.; Coles, S. J.; Seaton, C. C.; Schulze, E.; Lorenz, H.; Seidel-Morgenstern, A.; Stein, M.; Price, S. L. Are the Crystal Structures of Enantiopure and Racemic Mandelic Acids Determined by Kinetics or Thermodynamics? *J. Am. Chem. Soc.* **2015**, *137* (34), 11095−11104.
(30) Le Minh, T.; Von Langermann, J.; Lorenz, H.; Seidel-Morgenstern, A. Enantiomeric 3-Chloromandelic Acid System: Binary Melting Point Phase Diagram, Ternary Solubility Phase Diagrams and Polymorphism. *J. Pharm. Sci.* **2010**, *99* (9), 4084−4095.
(31) Leclercq, M.; Collet, A.; Jacques, J. Etude des Melanges d'Antipodes Optiques - XII. *Tetrahedron* **1976**, *32*, 821−828.
(32) Paukov, I. E.; Kovalevskaya, Y. A.; Boldyreva, E. V. Low-temperature heat capacity of L- and DL-phenylglycines. *J. Therm. Anal. Calorim.* **2012**, *108* (3), 1311−1316.
(33) Paukov, I. E.; Kovalevskaya, Y. A.; Boldyreva, E. V. Low-temperature thermodynamic properties of L- and DL-valines. *J. Therm. Anal. Calorim.* **2013**, *111* (1), 905−910.
(34) Drebushchak, V. A.; Kovalevskaya, Y. A.; Paukov, I. E.; Boldyreva, E. V. Heat capacity of D- and DL-serine in a temperature range of 5.5 to 300 K. *J. Therm. Anal. Calorim.* **2007**, *89* (2), 649−654.
(35) Makhatadze, G. I. Heat capacities of amino acids, peptides and proteins. *Biophys. Chem.* **1998**, *71* (2−3), 133−156.
(36) Paukov, I. E.; Kovalevskaya, Y. A.; Boldyreva, E. V. Low-temperature thermodynamic properties of L-cysteine. *J. Therm. Anal. Calorim.* **2008**, *93* (2), 423−428.
(37) Paukov, I. E.; Kovalevskaya, Y. A.; Boldyreva, E. V. Low-temperature thermodynamic properties of dl-cysteine. *J. Therm. Anal. Calorim.* **2010**, *100* (1), 295−301.
(38) Wang, Y. L.; LoBrutto, R.; Wenslow, R. W.; Santos, I. Eutectic composition of a chiral mixture containing a racemic compound. *Org. Process Res. Dev.* **2005**, *9* (5), 670−676.
(39) Otero-de-la-Roza, A.; Cao, B. H.; Price, I. K.; Hein, J. E.; Johnson, E. R. Predicting the Relative Solubilities of Racemic and Enantiopure Crystals by Density-Functional Theory. *Angew. Chem., Int. Ed.* **2014**, *53* (30), 7879−7882.
(40) Dunitz, J. D.; Gavezzotti, A. Molecular recognition in organic crystals: Directed intermolecular bonds or nonlocalized bonding? *Angew. Chem., Int. Ed.* **2005**, *44* (12), 1766−1787.
(41) Dunitz, J. D.; Gavezzotti, A. How molecules stick together in organic crystals: weak intermolecular interactions. *Chem. Soc. Rev.* **2009**, *38* (9), 2622−2633.
(42) Erdemir, D.; Lee, A. Y.; Myerson, A. S. Nucleation of Crystals from Solution: Classical and Two-Step Models. *Acc. Chem. Res.* **2009**, *42* (5), 621−629.
(43) Nangia, A. Conformational polymorphism in organic crystals. *Acc. Chem. Res.* **2008**, *41* (5), 595−604.
(44) Cruz-Cabeza, A. J.; Bernstein, J. Conformational Polymorphism. *Chem. Rev.* **2014**, *114* (4), 2170−2191.
(45) Nyman, J.; Day, G. M. Static and lattice vibrational energy differences between polymorphs. *CrystEngComm* **2015**, *17* (28), 5154−5165.
(46) Day, G. M.; Price, S. L.; Leslie, M. Atomistic calculations of phonon frequencies and thermodynamic quantities for crystals of rigid organic molecules. *J. Phys. Chem. B* **2003**, *107* (39), 10919−10933.
(47) Abdulla, M.; Refson, K.; Friend, R. H.; Haynes, P. D. A first-principles study of the vibrational properties of crystalline tetracene under pressure. *J. Phys.: Condens. Matter* **2015**, *27* (37), 375402.
(48) Červinka, C.; Fulem, M.; Stoffel, R. P.; Dronskowski, R. Thermodynamic Properties of Molecular Crystals Calculated within the Quasi-Harmonic Approximation. *J. Phys. Chem. A* **2016**, *120* (12), 2022−2034.
(49) Using CASTEP and the PBE-TS functional, we were unable to converge free energy differences between different cells without having any imaginary frequencies within the Brillouin zone for all crystals. Full periodic electronic structure methods are very challenging to apply to small molecular crystals because of the potential energy surface varying from shallow intermolecular interactions to steep covalent bonds.
(50) In the case of no enantiomeric excess, eq 3 gives $x_{eu} = 0.5$, and $\alpha_{min} = 2$ and the Gibbs free energy of solution difference is then $\Delta_{RS\text{-}S}\Delta G_{sol} = -RT \ln(2)$, corresponding to an ideal conglomerate, a mechanical mixture of both enantiopure crystals. With the alternative reference state this limiting case corresponds to an energy difference of 0 kJ mol^{-1} (see Supporting Information, section A).
(51) Palmer, D. S.; McDonagh, J. L.; Mitchell, J. B. O.; van Mourik, T.; Fedorov, M. V. First-Principles Calculation of the Intrinsic Aqueous Solubility of Crystalline Druglike Molecules. *J. Chem. Theory Comput.* **2012**, *8* (9), 3322−3337.
(52) Gavezzotti, A. *Theoretical Aspects and Computer Modeling of the Molecular Solid State*; Wiley and Sons: Chichester, 1997.
(53) Brandenburg, J. G.; Grimme, S. Accurate Modeling of Organic Molecular Crystals by Dispersion-Corrected Density Functional Tight Binding (DFTB). *J. Phys. Chem. Lett.* **2014**, *5* (11), 1785−1789.
(54) Otero-de-la-Roza, A.; Johnson, E. R. A benchmark for non-covalent interactions in solids. *J. Chem. Phys.* **2012**, *137* (5), 054103.
(55) Reilly, A. M.; Tkatchenko, A. Understanding the role of vibrations, exact exchange, and many-body van der Waals interactions in the cohesive properties of molecular crystals. *J. Chem. Phys.* **2013**, *139* (2), 024705−024705.
(56) Price, S. L.; Leslie, M.; Welch, G. W. A.; Habgood, M.; Price, L. S.; Karamertzanis, P. G.; Day, G. M. Modelling organic crystal structures using distributed multipole and polarizability-based model intermolecular potentials. *Phys. Chem. Chem. Phys.* **2010**, *12* (30), 8478−8490.
(57) Nyman, J.; Pundyke, O. S.; Day, G. M. Accurate force fields and methods for modelling organic molecular crystals at finite temperatures. *Phys. Chem. Chem. Phys.* **2016**, *18* (23), 15828−15837.

DOI: 10.1021/acs.cgd.7b00582
Cryst. Growth Des. 2017, 17, 4676−4686

(58) Pascale, F.; Zicovich-Wilson, C. M.; López Gejo, F.; Civalleri, B.; Orlando, R.; Dovesi, R. The calculation of the vibrational frequencies of crystalline compounds and its implementation in the CRYSTAL code. *J. Comput. Chem.* **2004**, *25* (6), 888−897.
(59) Le Parlouër, P. Simultaneous TG-DSC: a new technique for thermal analysis. *Thermochim. Acta* **1987**, *121*, 307−322.
(60) Ditmars, D. A.; Ishihara, S.; Chang, S. S.; Bernstein, G. Measurement of the relative enthalpy of pure a-Al2O3 (NBS heat capacity and enthalpy Standard Reference Material No. 720) from 273 to 1173. *Journal of Research of the National Bureau of Standards* **1982**, *87*, 159−163.
(61) Robie, R. A.; Hemingway, B. *Apparatus and Methods for Low Temperature Heat Capacity Measurements. The Heat Capacity of Standard Benzoic Acid. Geological Survey Professional Paper* 1972, 755.
(62) Le Minh, T.; Lorenz, H.; Seidel-Morgenstern, A. Enantioselective Crystallization Exploiting the Shift of Eutectic Compositions in Solid-Liquid Phase Diagrams. *Chem. Eng. Technol.* **2012**, *35* (6), 1003−1008.
(63) Le Minh, T. Designing crystallization based-enantiomeric separation for chiral compound-forming systems in consideration of polymorphism and solvate formation. Ph.D. Thesis, Otto-von-Guericke University Magdeburg, 2014.
(64) Lebedev, B. V.; Kulagina, T. G.; Kiparisova, E. G. The thermodynamic properties of L-lactide in the temperature range 0−430 K. *Zh. Fiz. Khim.* **1999**, *73* (4), 609−616.
(65) Emel'yanenko, V. N.; Verevkin, S. P.; Pimerzin, A. A. The thermodynamic properties of DL- and L-lactides. *Russian Journal of Physical Chemistry A* **2009**, *83* (12), 2013−2021.
(66) Sure, R.; Grimme, S. Corrected small basis set Hartree-Fock method for large systems. *J. Comput. Chem.* **2013**, *34* (19), 1672−1685.
(67) Del Ben, M.; Hutter, J.; VandeVondele, J. Second-Order Møller−Plesset Perturbation Theory in the Condensed Phase: An Efficient and Massively Parallel Gaussian and Plane Waves Approach. *J. Chem. Theory Comput.* **2012**, *8* (11), 4177−4188.
(68) Dovesi, R.; Orlando, R.; Erba, A.; Zicovich-Wilson, C. M.; Civalleri, B.; Casassa, S.; Maschio, L.; Ferrabone, M.; De La Pierre, M.; D'Arco, P.; Noel, Y.; Causa, M.; Rerat, M.; Kirtman, B. CRYSTAL14: A Program for the Ab Initio Investigation of Crystalline Solids. *Int. J. Quantum Chem.* **2014**, *114* (19), 1287−1317.
(69) Aradi, B.; Hourahine, B.; Frauenheim, T. DFTB+, a Sparse Matrix-Based Implementation of the DFTB Method†. *J. Phys. Chem. A* **2007**, *111* (26), 5678−5684.
(70) Grimme, S.; Antony, J.; Ehrlich, S.; Krieg, H. A consistent and accurate ab initio parametrization of density functional dispersion correction (DFT-D) for the 94 elements H-Pu. *J. Chem. Phys.* **2010**, *132* (15), 154104.
(71) Ahlrichs, R.; Bar, M.; Haser, M.; Horn, H.; Kolmel, C. Electronic-Structure Calculations on Workstation Computers - the Program System Turbomole. *Chem. Phys. Lett.* **1989**, *162* (3), 165−169.
(72) Kazantsev, A. V.; Karamertzanis, P. G.; Adjiman, C. S.; Pantelides, C. C. Efficient Handling of Molecular Flexibility in Lattice Energy Minimization of Organic Crystals. *J. Chem. Theory Comput.* **2011**, *7* (6), 1998−2016.
(73) Klamt, A. Conductor-Like Screening Model for Real Solvents - a New Approach to the Quantitative Calculation of Solvation Phenomena. *J. Phys. Chem.* **1995**, *99* (7), 2224−2235.
(74) Kulagina, T. G.; Lebedev, Y. G.; Lyudvig, Y. B.; Barskaya, I. G.; Kiparisova, Ye. B. Thermodynamics of dl-Lactide, Polylactide and Polymerization of DL-Lactide in the range of 0−430 K. *Polym. Sci. U.S.S.R.* **1982**, *24* (7), 1702−1708.
(75) Neau, S. H.; Bhandarkar, S. V.; Hellmuth, E. W. Differential Molar Heat Capactities to Test Ideal Solubility Estimations. *Pharm. Res.* **1997**, *14* (5), 601−605.
(76) de Barros, T. M. V. R.; Santos, R. C.; Fernandes, A. C.; da Piedade, M. E. M. Accuracy and precision of heat capacity measurements using a heat flux differential scanning calorimeter. *Thermochim. Acta* **1995**, *269−270*, 51−60.
(77) Quantum Design, San Diego, CA.
(78) Ravikumar, K.; Rajan, S. S.; Pattabhi, V.; Gabe, E. J. Structure of Naproxen, C14h14o3. *Acta Crystallogr., Sect. C: Cryst. Struct. Commun.* **1985**, *41* (2), 280−282.
(79) Donahue, M.; Botonjic-Sehic, E.; Wells, D.; Brown, C. W., Understanding Infrared and Raman Spectra of Pharmaceutical Polymorphs. *Am. Pharmaceut. Rev.* **2011**, *14*, (2).
(80) Yang, J.; Hu, W. F.; Usvyat, D.; Matthews, D.; Schutz, M.; Chan, G. K. L. Ab initio determination of the crystalline benzene lattice energy to sub-kilojoule/mol accuracy. *Science* **2014**, *345* (6197), 640−643.
(81) Docherty, R.; Pencheva, K.; Abramov, Y. A. Low solubility in drug development: de-convoluting the relative importance of solvation and crystal packing. *J. Pharm. Pharmacol.* **2015**, *67* (6), 847−856.
(82) D'Oria, E.; Karamertzanis, P. G.; Price, S. L. Spontaneous Resolution of Enantiomers by Crystallization: Insights from Computed Crystal Energy Landscapes. *Cryst. Growth Des.* **2010**, *10* (4), 1749−1756.
(83) Grimme, S.; Hansen, A.; Brandenburg, J. G.; Bannwarth, C. Dispersion-Corrected Mean-Field Electronic Structure Methods. *Chem. Rev.* **2016**, *116* (9), 5105−5154.
(84) Beran, G. J. O. Modeling Polymorphic Molecular Crystals with Electronic Structure Theory. *Chem. Rev.* **2016**, *116* (9), 5567−5613.
(85) Gray, A. E.; Day, G. M.; Leslie, M.; Price, S. L. Dynamics in crystals of rigid organic molecules: contrasting the phonon frequencies calculated by molecular dynamics with harmonic lattice dynamics for imidazole and 5-azauracil. *Mol. Phys.* **2004**, *102* (9−10), 1067−1083.
(86) All of the compounds in this study show similarly high values of x_{eu}. The same variability of x_{eu} in different solvent, the presence and absence of a eutectic shift is found for other chiral systems having lower eutectic compositions. These systems would be more sensitive to changes in the free energy difference, Supporting Information, Figure S2.
(87) Brandel, C.; Cartigny, Y.; Coquerel, G.; ter Horst, J. H.; Petit, S. Prenucleation Self-Assembly and Chiral Discrimination Mechanisms during Solution Crystallisation of Racemic Diprophylline. *Chem. - Eur. J.* **2016**, *22* (45), 16103−16112.

DOI: 10.1021/acs.cgd.7b00582
Cryst. Growth Des. 2017, 17, 4676−4686